Eur. Phys. J. B **19**, 363–373 (2001)

THE EUROPEAN PHYSICAL JOURNAL B

EDP Sciences

Temperature and pressure dependencies of the crystal structure of the organic superconductor $(TMTSF)_2ClO_4$

D. Le Pévelen[1], J. Gaultier[1], Y. Barrans[1], D. Chasseau[1,a], F. Castet[2], and L. Ducasse[2]

[1] Groupe des Sciences Moléculaires[b], Institut de Chimie de la Matière Condensée de Bordeaux, 33608 Pessac Cedex, France
[2] Laboratoire de Physico-Chimie Moléculaire[c], Université Bordeaux I, 33405 Talence Cedex, France

Received 10 April 2000 and Received in final form 27 September 2000

Abstract. The crystal structure of $(TMTSF)_2ClO_4$ has been determined at (7 K, 1 bar) and at (7 K, 5 kbar) with a high accuracy. For the latter, low temperature and pressure were applied simultaneously using a X-ray diffraction instrumentation designed in our laboratory, these results are the first for molecular compounds. The effects of lowering the temperature are not the same as those produced by increasing the pressure. At (7 K, 1 bar) the anion ordering which occurs in this compound, and which is characterised by the appearance of $b^*/2$ superlattice reflections, is well observed. This anion ordering leads to the presence of two independent stacks of TMTSF cations which is the only case found in the Bechgaard salts family. The comparison of the low temperature crystal structures under atmospheric pressure and at 5 kbar shows that the centres of mass are nearly the same, independent of the pressure: the interchain interactions do not depend on the doubling of the unit cell. Under pressure, the ordering (0, 1/2, 0) does not occur at any temperature. These structural data are confirmed by the quantum chemical calculations which show that the difference in the site energy of the two independent cations is 100 meV.

PACS. 61.50.Ks Crystallographic aspects of phase transformations; pressure effects – 74.70.Kn Organic superconductors – 71.15.Fv Atomic- and molecular-orbital methods (including tight binding approximation, valence-bond method, etc.)

1 Introduction

The quasi-one dimensional $(TMTSF)_2X$ salts, where TMTSF = tetramethyltetraselenafulvalene, present a wide variety of physical properties such as superconductivity, metallic and insulating behaviours, for a review see [1–3]. Among the numerous compounds of this family, $(TMTSF)_2ClO_4$ is one of the most remarkable. Indeed, it is the only TMTSF salt which becomes a superconductor at low temperature (2 K) and ambient pressure [4]. A transition which corresponds to the anion ordering with wave vector $q = (0, 1/2, 0)$ [5,6] is observed at 24 K. If the cooling rate is too fast, neither the order-disorder transition nor the superconducting state are observed [6,7]. In this case, the ground state of $(TMTSF)_2ClO_4$ is insulating [8]. The room temperature structure of this salt was investigated previously [9]. The TMTSF units are nearly planar and they stack along the a cell axis. Within a column, TMTSF units repeat by inversion leading to zig-zag type stacking. The TMTSF columns form ab sheets spaced by anions. The ClO_4^- anions are located at the inversion centre of the unit cell and thus they are statistically disordered.

Under pressure, the superconducting transition temperature decreases rapidly [10,11], as frequently seen in organic compounds, till at 5 kbar, the transition temperature is about 50 mK [11]. The effect of pressure on the temperature of the anion ordering is the subject of a continuing debate. Early resistivity measurements [10] showed at a maximum pressure of 8 kbar, a change of slope at $T = 25$ K. This change was ascribed to the existence of the perchlorate ordering. More recent measurements [12] analysed the temperature dependence of the resistance along the c^* direction as a function of pressure up to $P = 40$ kbar, by means of an extremely careful control of the rate of slow cooling (<5 K h^{-1}). For a better determination of the transition temperature, the derivative of the resistance *vs.* T was calculated. The relative variation of the derivative, $(1/\rho)\Delta(\mathrm{d}\rho/\mathrm{d}T)$, is chosen as a measurement of the "strength" of the transition. The results clearly show two regions. For pressure less than 6 kbar, this "strength" is high but decreases rapidly; while at high pressure, this "strength" is quite low (less than 10% than the 0.2 kbar value). Moreover, in the first region, the ordering temperature remains constant while it increases up to 41 K at 11 kbar. Magnetoresistance measurements allowed

[a] e-mail: chasseau@icmcb.u-bordeaux.fr
[b] UPR CNRS 9048
[c] UMR 5803

Kang *et al.* [13] to determine the (P, T, H) phase diagram for $(TMTSF)_2ClO_4$ using a cooling rate of 7 mK min^{-1} through the anion transition region to achieve a well relaxed state. The perchlorate phase diagram has two pressure domains of an anion ordered phase and a non ordered phase. The separation line at $P = 4$ kbar corresponds to the loss of superconductivity at $H = 0$, and to the different characteristics of the FISDW states. The same kind of measurements were also performed on $(TMTSF)_2PF_6$. They show that the crossover between the SDW phase and the SC phase occurs at $P = 6$ kbar. The critical pressure was first measured as $P = 9$ kbar [14]. It is now recognised that the pressure values of the Orsay group (1985) should be reduced by a factor of approximately 1.5 units [12], giving $P = 5$ kbar for the maximum pressure at which the anion ordering is observed for the ClO_4 data. There is an overall agreement between the different maximum values for the pressure for the anion ordering if one notes that for $P > 6$ kbar, the strength of the anion ordering is very weak. This apparent discrepancy is the main motivation for determining the structural characteristics of this compound at low temperature or/and under pressure. The first low temperature structural results were obtained for $(TMTSF)_2ClO_4$ at ambient pressure by diffuse X-Ray scattering [5]. This study has revealed spots of wave vector (0, 1/2, 0) starting at 40 K, which condensate into superlattice reflections at 24 K. The intensities of these superlattice reflections depend on the cooling rate. Then, a low temperature (7 K) crystal structure was determined at ambient pressure using both X-Ray and neutron diffraction [15–17]. It confirmed the doubling of the unit cell along the b direction and the ordering of the anion. The very small number of superstructure reflections did not allow an accurate analysis of these results: the refinement was performed using the approximation of molecular rigid blocks, by imposing identical molecular geometry for the two crystallographically independent TMTSF.

The room temperature crystal structure of $(TMTSF)_2ClO_4$ was also determined [18] as a function of applied pressure. No structural transition was found in that case up to 10 kbar. Up to now, no structural data were known at low temperature and under pressure for this salt. In the family of the Bechgaard salts, the only example of simultaneously low T and high P crystal structure is $(TMTSF)_2PF_6$ using neutron diffraction [19]. To our knowledge, no X-ray crystal structure of a molecular conductor, and more generally of an organic compound, under these coupled constraints, has been published.

More recently, we have determined the low T or high P crystal structures of a large variety of mainly BEDT-TTF derivatives using proprietary instrumentation [20]. We have improved this instrumentation and have modified it to collect X-ray data simultaneously under hydrostatic pressure and low temperature. Using this technique, we have investigated the low temperature (7 K) crystal structures of $(TMTSF)_2ClO_4$ at 1 bar and 5 kbar. From these results, the transfer integrals, the band structures and the Fermi surfaces were calculated. The influence of pressure and temperature on the anion ordering and, consequently, on the TMTSF moieties and packing, will be discussed in detail.

2 Experimental

2.1 X-ray crystallography

2.1.1 Apparatus

The diffractometer used to collect the crystal data at low temperature and under atmospheric (LT) or hydrostatic (5 kbar) pressure (HPLT) is a three-circle diffractometer specially designed in our laboratory [20]. This diffractometer uses normal beam geometry with graphite monochromatised MoKα radiation. Low temperatures down to 7 K are obtained by means of a closed-cycle helium cryostat to an accuracy of 0.3 K. The sample is mounted on a brass tip which is placed on the cold finger of the cryostat. The sample is then sealed in a beryllium can containing He exchange gas. The whole assembly is then surrounded by a radiation shield and the beryllium vacuum shroud.

The diamond anvil with a beryllium gasket pressure cell used in our laboratory was described previously [20]. This gasket was 1.0 mm thick unlike those used before (0.5 mm), which allowed us to use a crystal of larger dimensions and as a result to collect more intense reflections.

For the HPLT measurements, new enlarged beryllium cans were modified in order to allow the pressure cell to be fixed on the cold finger [21]. Prior to measurement, the quality of the secondary vacuum was checked at low temperature. The pressure was equalized at room temperature, before and after a temperature cycle.

2.1.2 Experimental data

Two pieces of the same crystal were used in the LT and HPLT experiments. The quality of the chosen crystal for the low temperature study was first checked by rotating-crystal and Weissenberg photographs. The observed reflections were strong and single. Reference checks were performed every 30 reflections. No significant variation of intensity was observed. The reflection intensities were corrected from the Lorentz and polarisation effects and a numerical absorption correction was applied.

For the LT measurements, over all the temperature range, the cooling rate was less than 2 K min^{-1} and about 1 K min^{-1} below 50 K and through the transition. At 7 K, superstructure reflections were observed. The intensities of two of these reflections were followed when increasing temperature: at 25 K, the intensity is equal to zero, which is in agreement with the previous results [5,6].

At 7 K, the unit cell parameters and an orientation matrix were obtained from accurately measured angles of 18 reflections: Table 1. Out of 3927 measured reflections, 1009 were superlattice reflections. After the data reduction, only 2691 reflections were considered as unique and

Table 1. Crystal and experimental data.

	LT	HPLT
cryst. dim. (mm^3)	$1.50 \times 0.10 \times 0.06$	$0.50 \times 0.125 \times 0.075$
space group	$P_{\bar{1}}$	$P_{\bar{1}}$
formula unit per cell	2	1
cell parameters	$a = 7.083\,(3)$ Å. $\alpha = 84.40°\,(1)$ $b = 15.334\,(2)$ Å. $\beta = 87.62°\,(1)$ $c = 13.182\,(4)$ Å. $\gamma = 69.00°\,(2)$	$a = 7.052\,(5)$ Å. $\alpha = 84.51°\,(2)$ $b = 7.620\,(8)$ Å. $\beta = 87.85°\,(2)$ $c = 13.125\,(6)$ Å. $\gamma = 69.20°\,(3)$
volume ($Å^3$)	1330	665
density ($g\,cm^{-3}$)	2.486	2.517
$\mu(mm^{-1})$	11.949	12.100
$F(000)$	930	465
radiation λ(Å)	Mo (0.71069)	Mo (0.71069)
$2\theta_{max}(°)$	53	50
$h,\ k,\ l$	$5,\ \pm18,\ \pm16$	$5,\ \pm9,\ \pm15$
absorption correction	numerical	numerical
reflections measured	3927 (1009 superstruct. refl.)	2785
unique reflections	3261	1963
criteria	$I \geq 3\sigma(I)$	$I \geq 5\sigma(I)$
reflections used	2691	1361
R_{int} (%)	1.3	1.15
$R(R_w)$ (%)	4.60, (4.90)	4.40, (3.90)
σ (Se-C,C-C;Cl-O), Å	0.010; 0.015; 0.009	0.011; 0.015; 0.015

observed ($I > 3\sigma(I)$). The LT unit cell contains two formula units, $(TMTSF)_2ClO_4$. The structure was refined starting from the atomic coordinates found at low temperature by Gallois [15]. The final values of the reliability factors are $R = 4.6\%$ and $Rw = 4.9\%$. The atomic thermal parameters were refined isotropically.

The HPLT experiment was performed, first by applying pressure (5 kbar) and then by cooling down to 7 K. At 5 kbar (295 K), the absence of $b^*/2$ superlattice reflections mentioned previously [18] was confirmed. The HPLT cell parameters and an orientation matrix were obtained from the measurements of the angular positions of 21 reflections. No $b^*/2$ superlattice reflections were found when measuring the intensities of the reflections corresponding to the $(a,\ 2b,\ c)$ unit cell. An ordering of the anions with a different wavevector is not excluded from this experiment. In order to check that this absence of reflections is not due to the pressure cell itself, the influence of the apparatus was examined under different temperature/pressure cycling process. After the data collection, the temperature was increased up to room temperature. The pressure was released down to ambient pressure and the temperature was decreased to 7 K with the crystal still in the pressure cell. The superstructure reflections were observed and finally disappear at 24 K with the increasing temperature, confirming that there is no influence of the pressure cell on the results. Out of 2785 measured reflections only 1361 were considered as unique and observed ($I > 5\sigma(I)$). The final R factors are $R = 4.4\%$ and $Rw = 3.9\%$. Crystal and experimental data are listed in Table 1.

2.2 Transfer integrals and band structure calculations

The band structures of organic compounds are quite commonly evaluated by means of the Extended Hückel Theory. It is not a self-consistent procedure and the dispersions do not depend on band filling. The EHT matrix elements are proportional to the overlaps between atomic orbitals. Apart from the single/double-ζ basis set type, the only parameters are the atomic ionisation potentials. This crude approximation was used by many authors [17,22–25]. This one-electron approach successfully reproduces the topology of the Fermi surface of metallic salts. For quasi-1D salts, the nesting of the Fermi lines is related to the occurrence of the Spin Density Wave state, and the calculated nesting vector [16] agrees with the observed SDW wavevector [26]. For 2D salts (as the BEDT-TTF derivatives of the β- and κ phases), the agreement between the shape and the location of the closed orbit of the calculated FS and the experimental data extracted from Angular Magneto-Resistance Oscillations is fairly good (for a review, see [2]).

A few *ab initio* band structures have been performed for metallic salts [27,28] using Density Functional Theory within the Local Density Approximation. In the case of $(TMTSF)_2ClO_4$ [27], it has been shown that the dispersions of the bands close to the Fermi level and the lines of the Fermi surface are very similar to the simple Extended Hückel results. This result comforts our approach based on a simple evaluation of the transfer integrals by means of Extended Hückel theory.

The transfer integrals are evaluated by means of the dimer-splitting approximation [29,30]. If one considers two molecules M1 and M2 represented by their frontier orbitals, $HOMO_1$ and $HOMO_2$ respectively, the bonding (Ψ^+, energy E^+) and the antibonding (Ψ^-, energy E^-) combinations of the dimer M1-M2 read:

$$\Psi^+ = c_1^+(\mathrm{HOMO}_1) + c_2^+(\mathrm{HOMO}_2)$$
$$\Psi^- = c_1^-(\mathrm{HOMO}_1) + c_2^-(\mathrm{HOMO}_2)$$

while the corresponding energies are:

$$E^+ = \frac{\Delta}{2} + \frac{K}{2} \quad ; \quad \frac{c_1^+}{c_2^+} = -\frac{\Delta}{2t} + \frac{K}{2t}$$
$$E^- = \frac{\Delta}{2} - \frac{K}{2} \quad ; \quad \frac{c_1^-}{c_2^-} = -\frac{\Delta}{2t} - \frac{K}{2t}$$

where t is the transfer integral, Δ is the difference between the energies of the orbitals $HOMO_1$ and $HOMO_2$ and $K = [\Delta^2 + 4t^2]^{1/2}\Delta$ is non zero only when M1 and M2 correspond to crystallographically independent molecules. The dimer splitting allows us to extract both t and Δ and the value of Δ must be similar to the value obtained from monomer calculations.

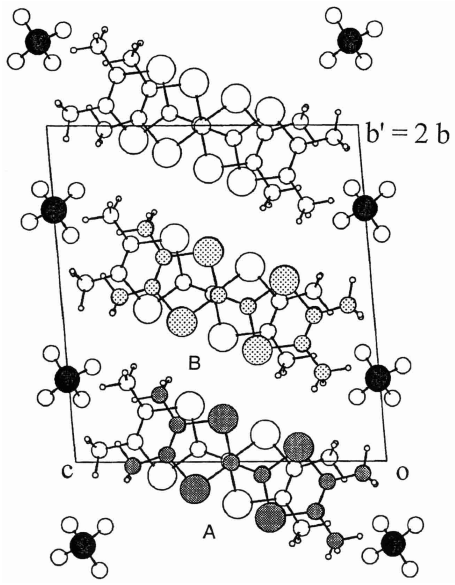

Fig. 1. View of the packing of $(TMTSF)_2ClO_4$ along the a axis at LT; the dark and grey symbols represent independent TMTSF cations.

3 Results[1]

3.1 Crystal structure

3.1.1 Crystal packing

The $(TMTSF)_2ClO_4$ salt crystallises in the $P\bar{1}$ space group independent of the physical conditions.

At RT, the unit cell contains two TMTSF cations and one anion. The TMTSF units are nearly planar and they stack along the a cell axis. Within a column, these units repeat by inversion leading to zig-zag type stacking. The tilt angle between the a cell axis and the normal to the TMTSF molecular plane is quite small ($\sim 2°$). The TMTSF columns form ab sheets spaced by anions. The ClO_4^- anions are located at the inversion centre of the unit cell and are statistically disordered and every oxygen atom occupies either of two sites with the same probability.

At LT (7 K), the presence of the superlattice reflections of wavevector (0, 1/2, 0) leads to the doubling of the b parameter. This corresponds to an ordering of the ClO_4^- anions along the b direction and to the existence of two kinds (noted A and B) of independent cationic columns. A view along the a axis is shown in Figure 1.

At HPLT (7 K, 5 kbar), no superlattice reflection involving a doubling of the b unit cell parameter was observed. The general characteristics of the RT crystal packing are preserved (Fig. 2). The inorganic anion ClO_4^- is still disordered.

[1] The atomic coordinates and thermal motion parameters for the LT, HP and HPLT crystal structures may be obtained upon request from the authors.

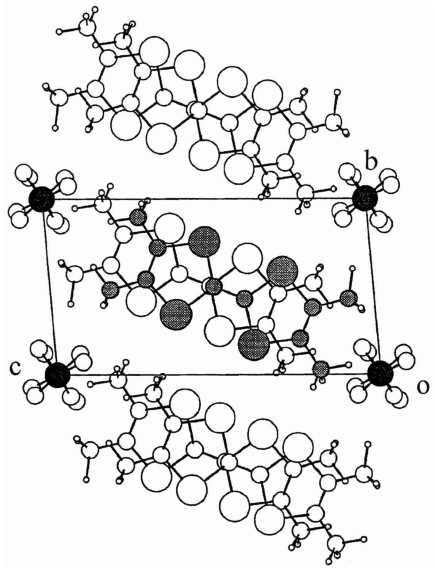

Fig. 2. View of the packing of $(TMTSF)_2ClO_4$ along the a axis at HPLT.

The relative variations of the unit cell volumes under the applied constraints, $\Delta V/V$ are: -5% from RT to LT under atmospheric pressure, -5% from atmospheric pressure to 5 kbar at room temperature and -0.5% from 300 K to 7 K at 6 kbar. These variations are quite anisotropic: in every case, the relative variation of the unit cell parameter a amounts to about 50% of $\Delta V/V$. The $\Delta b/b$ variation is twice as large under pressure as that produced by decreasing the temperature down to 7 K.

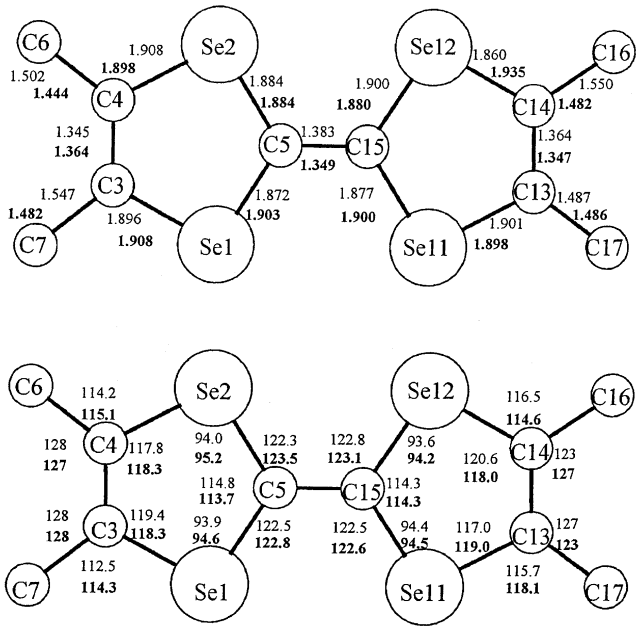

Fig. 3. Bond lengths (Å) and angles (°) of the A and B TMTSF cations at LT. The values for B are given in boldface.

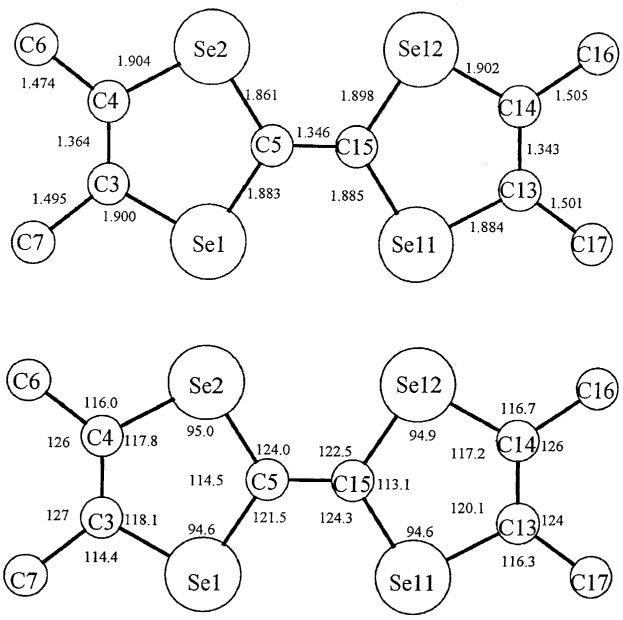

Fig. 4. Bond lengths (Å) and angles (°) of the TMTSF cation at HPLT.

3.1.2 TMTSF cation conformation and anion conformation

The LT bond lengths and angles for the two independent cations A and B in the LT structure are reported in Figure 3. The LT standard deviations of the bond lengths are almost identical to the RT value (∼0.01−0.02 Å). The deviation from the ideal D_{2h} symmetry of the cation is the same for the two independent cations for the C-Se distances and it is maximum for the $C_{external}$-Se and C-CH_3 distances (∼0.03 Å). This dispersion is slightly larger than for the RT data.

The difference between the two independent cations comes mainly from the methyl groups. The average of the C-CH_3 distances is 1.52 Å for the A cation and 1.47 Å for the B cation while the $C_{external}$-Se distances average to 1.89 Å and 1.91 Å respectively.

The mean molecular planes have been calculated from the positions of the 6 central atoms. Using this definition, one finds that the deviation from the planarity for both A and B cations is close to the RT result although it is slightly larger for A than for B.

Of the mean plane of each five-membered group, some differences are observed between cations A and B. These groups are strictly planar in B, like at 295 K, but not in A. In the latter case, the carbon atoms of the methyl groups move away noticeably from the mean planes on opposite sides: C_6−0.12 Å and C_7−0.07 Å ; C_{16}+0.05 Å and C_{17}+ 0.12 Å, so, the A TMTSF adopts a chair-like conformation while the B cation is strictly planar.

The conformation of the TMTSF cation at HPLT (Fig. 4) is nearly the same as at HP [18]. The dispersion on chemically equivalent bonds is small. It is slightly smaller than the LT values. The TMTSF cation planarity is similar to the B cation planarity at LT. In particular, the carbon atoms of methyl groups belong to the mean plane of the five-membered rings.

Table 2. Bond lengths (Å) and angles (°) of the anion.

	LT	HPLT
Cl-O_{21}	1.44 (1)	1.47 (2)
Cl-O_{22}	1.42 (1)	1.36 (2)
Cl-O_{23}	1.45 (1)	1.42 (2)
Cl-O_{24}	1.47 (1)	1.53 (2)
O_{21}-Cl-O_{22}	109.5 (5)	111.3 (5)
O_{21}-Cl-O_{23}	109.7 (5)	109.3 (5)
O_{21}-Cl-O_{24}	108.4 (5)	103.7 (5)
O_{22}-Cl-O_{23}	112.0 (5)	116.1 (5)
O_{22}-Cl-O_{24}	109.3 (5)	110.4 (5)
O_{23}-Cl-O_{24}	107.9 (5)	105.2 (5)

In all structures except for the LT, the ClO_4^- anion is disordered. In these cases, the Cl atom is located on the centre of symmetry. The high value of the Cl Debye-Waller factor (which is twice as large as the Se or C values) suggests that the real position of the Cl atom is slightly displaced from this position. This observation may explain why the HPLT bond lengths and bond angles reported in Table 2 are characteristic of an irregular anion.

In the LT structure, the disorder of the anion disappears as the anions are not located on an inversion centre anymore. Moreover, they are not on the previous symmetry centre: the Cl atom is located 0.09 Å apart from this position. The LT conformation is quasi regular (Tab. 2).

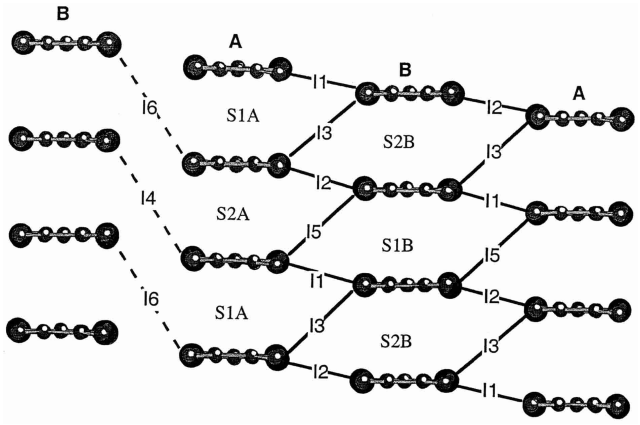

Fig. 5. LT cation-cation interactions: projection of the structure along the long molecular axis.

The dispersion is weak: 0.05 Å on bond lengths and less than 2° on angles.

3.1.3 Cation-cation interactions

In all structures except for the LT, as there is only one independent cation per unit cell, there are two overlap interactions (S_1 and S_2) and four types of interchain interactions (I_1, I_2, I_3 and I_4). The interactions between neighbouring cations are shown schematically in Figure 5 for the LT structure. There are two sets of intrachain interactions (noted S_{1A}, S_{2A}, S_{1B}, S_{2B}) and the I_3 and I_4 interactions are splitted so that I_5 and I_6 are also defined.

The transfer integrals are in Table 3 for the RT, HP, LT and HPLT crystal structures. In the case of the LT structure, the high degree of the structural determination allows us to quantify the energy difference Δ between the stacks A and B. We find that Δ is close to 100 meV (the site energy of A is higher than B).

The increase of the intrastack transfer integrals by the lowering T and/or increasing P had already been observed in organic salts. The transfer integral dimerisation ratio S_1/S_2 allows us to better discriminate between the effects of the different constraints. At 300 K, this ratio is not modified under pressure. At ambient pressure, the dimerisation ratio is slightly decreased from 1.17 to 1.12 by lowering T, according to the results of Gallois *et al.* which do not take into account the existence of 2 independent TMTSF. Under pressure, a similar decrease from 1.17 to 1.09 is observed. The main result of this calculation concerns the refined LT structure. As discussed above, the ClO_4 ordering along the b direction implies that the cations in neighbouring stacks might be different. The dimerisation ratio is strikingly different for the two stacks and its evolution is also different: it increases for the A column while it decreases for the B column. These ratios may be compared to the case of $(TMTSF)_2PF_6$ at low T for which the dimerisation is 1.07, very close to the B-value.

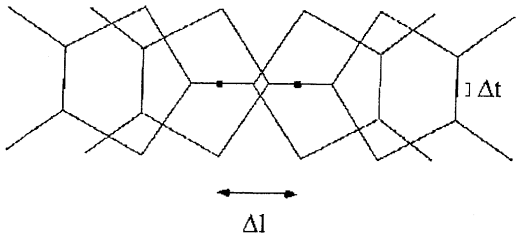

Fig. 6. Definition of the intrachain parameters Δl and Δt.

A quantitative analysis of the intrachain interaction is generally performed from the 3 geometrical parameters: the interplanar distance d, the transverse displacement Δt of the centres of the cations perpendicular to the long molecular axis and the longitudinal displacement Δl (Fig. 6). Other ways to measure these interactions are by comparing the distance between the centres of mass, Dm, or by averaging the 6 shortest Se-Se distances, noted $\langle d_{Se} \rangle$ (Table 4). The geometrical dimerisation ratio is defined as the ratio of Dm_2 to Dm_1 or of $\langle d_{Se} \rangle 2$ to $\langle d_{Se} \rangle 1$. These ratios are almost constant and close to 1. They show a tendency to decrease slightly under constraint. The ratio of the $\langle d_{Se} \rangle$ values shows a larger variation than the Dm results. It is concluded that these results are related to a deformation of the central part of the cation.

In order to obtain a more quantitative analysis of the interchain interaction effects, we performed different model calculations. First, the A transfer integrals were calculated by assigning to the A dimers the (d, Δl, Δt) of the B-stack (see Tab. 4). The integrals S_{1A} and S_{2A} now become S_{1A} (B-stack) = 399 meV and S_{2A} (B-stack) = 313 meV: the ratio of 1.27 has not changed. Second: as the molecular deformation is directly related to the Δ term, we have shown the effects of this term on the dimerisation by modeling the S_{1A} and the S_{2A} interactions using the geometry of the TMTSF cation of the B stack for each A cation while keeping the intermolecular parameters (d, Δl, Δt) of the real A stack. The model integrals are: S_{1A}(B-cation) = 355 meV and S_{2A}(B-cation) = 310 meV. The dimerisation ratio is now: $(S_1/S_2)_{A(B\text{-mol})} = 1.14$ *vs.* $(S_1/S_2)_B = 1.08$.

The large dimerisation of the transfer integrals in A stack, in comparison to B stack, is clearly a result of the molecular deformation and of the non zero difference in the site energy between A and B. For an hypothetical LT structure built of B cations only, the ratios average to 1.11, which is similar to the result found for the previous LT structure [17].

At room temperature, the transfer integrals increase under pressure but their ratio is not changed. At low T, pressure mainly changes S_2, which leads to a reduction of the dimerisation ratio. The HPLT data can be compared to the B stack values: the integrals slightly increase but the ratio remains the same. The effects of pressure, which prevents the anion ordering even at low T, do not allow the occurrence of two independent stacks, the TMTSF cation at HPLT being very similar to the B cation.

Table 3. Intrachain and interchain transfer integrals (meV). The transfer integrals for the crystal structures of references [9,17,18] were recalculated using the same parameters as in the present work.

	RT		LT		HP	HPLT
Ref.	[9]	[17]	this work		[18]	this work
			Mol A	Mol B		
S_1	350	392	413	362	372	376
S_2	299	349	324	335	318	346
S_1/S_2	1.17	1.12	1.27	1.08	1.17	1.09
I_1	−29	−52	−50		−37	−50
I_2	−58	−100	−100		−76	−101
$I_3(/I_5)$	55	64	70/71		65	65
$I_4(/I_6)$	13	21	20/21		17	20

Table 4. Parameters determining the intrachain overlaps (Å): for RT, HP, HPLT, the interaction S_1 is between the cation I and $(-I+b+c)$ and the interaction S_2 is between the cation I and $(-I+a+b+c)$; for LT: S_{1A} = A and $(-A+c)$, S_{2A} = A and $(-A+a+c)$; S_{1B} = B and $(-B+b+c)$, S_{2B} = B and $(-B+a+b+c)$.

	RT		LT		HP	HPLT
Ref.	[9]	[17]	this work		[18]	this work
			Mol A	Mol B		
d_1	3.63	3.52	3.55	3.55	3.55	3.54
Δl_1	1.483	1.44	1.399	1.440	1.455	1.397
Δt_1	0.066	0.02	0.086	−0.037	0.021	0.004
Dm_1	3.922	3.80	3.817	3.831	3.837	3.806
$\langle d_{Se}\rangle_1$	3.975	3.91	3.906	3.906	3.917	3.893
d_2	3.63	3.56	3.53	3.53	3.55	3.52
Δl_2	1.683	1.61	1.618	1.663	1.642	1.599
Δt_2	−0.018	0.02	−0.031	−0.035	−0.061	−0.063
Dm_2	4.001	3.91	3.883	3.902	3.912	3.867
$\langle d_{Se}\rangle_2$	4.010	3.89	3.910	3.913	3.937	3.894
Dm_2/Dm_1	1.022	1.029	1.017	1.018	1.019	1.016
$\langle d_{Se}\rangle_2/\langle d_{Se}\rangle_1$	1.009	0.995	1.001	1.002	1.005	1.000

A comparison of the effect of pressure on the ClO_4 and the PF_6 salts shows a different behaviour. The mean intrastack integral, $(S_1+S_2)/2$, varies from 325 meV (RT) to 361 meV (HPLT) for ClO_4, while for PF_6 it varies from 315 meV (RT) to 370 meV (HPLT) [21]. Although the HPLT ratios are the same for both salts, the pressure dependence of the RT values is quite different. It remains constant (1.17) for ClO_4 while it varies from 1.23 to 1.07 for PF_6. For ClO_4, the decrease is only due to temperature while, for PF_6, it is only due to pressure.

The variations of the interchain transfer integrals upon the different constraints are also gathered in Table 3. The ratio of the intrachain integrals to the interchain transfer ones gives a measure of the quasi-1D dimensional character of the Bechgaard salts. The 2D character is reinforced by decreasing the temperature and/or increasing the pressure. The effect of T and/or P induces much larger variations of I_1 and I_2 compared to I_3 and I_4.

At ambient pressure, the effect of lowering T induces quite a large increase of the interactions, with almost a doubling of I_1 and I_2 values. The anion ordering does not change the interchain interactions, by comparing I_3 and I_5, I_4 and I_6, and these values are almost identical to those found previously [17].

The pressure dependence of these integrals (HP) is less pronounced than the temperature variation (LT) and the enhancement of I_1 and I_2 *vs.* I_3 and I_4 is weaker. At HP, and decreasing T, I_1 and I_2 increase while I_3 and I_4 remain the same so that the HPLT results are identical to the LT integrals. These results are consistent with those obtained from the PF_6 compound, although the interchain interactions are always weaker in PF_6 compared to ClO_4. The main difference between the ClO_4 and the PF_6 salts are the variations under T and/or P of the intrachain integrals. We have concluded that the ClO_4 salt presents a more pronounced 2D character than the PF_6 salt at HPLT.

As discussed in previous papers [16], the interchain integrals depend not only on the shortest intermolecular Se-Se distances (noted d_i for each I_i interaction) but also

Table 5. The shortest Se...Se interchain contacts d_i(Å) and the corresponding ϕ_i angles (°).

	RT	LT		HP	HPLT
Ref.	[9]	[17]	this work	[18]	this work
d_1	3.778	3.560	3.606	3.654	3.596
ϕ_1	17.5	13.9	14.6	17.1	14.6
d_2	3.865	3.730	3.730	3.737	3.711
ϕ_2	16.7	12.5	13.4	16.0	13.2
d'_2	3.955	3.790	3.802	3.851	3.789
ϕ'_2	15.4	11.9	12.0	14.0	13.1
$d_3(/d_5)$	4.192	4.210	4.206/4.222	4.115	4.188
$\phi_3(/\phi_5)$	36.8	40.5	39.0/39.4	37.8	39.1
$d_4(/d_6)$	5.827	5.460	5.476/5.505	5.639	5.479
$\phi_4(/\phi_6)$	54.6	52.2	54.1/53.0	54.7	53.6

on the angles ϕ_i (the ϕ angle is defined as the angle between the direction of Se...Se atoms and the mean plane of the TMTSF cation). These angles take into account the competition between the π-π type overlap and the σ-σ type one. When ϕ is small, the π-π interaction dominates, so that t_I is negative: this is the case of I_1 and I_2. Larger values of ϕ correspond to σ-σ interaction and positive t_I as in the case of I_3 and I_4. The values of the geometrical parameters for the ClO_4 salt are collected in Table 5. The angles ϕ_1 and ϕ_2 decrease while the angle ϕ_3 increases independent of the constraints. These effects are much more pronounced when T is lowered: the variation is about 3° for LT or HPLT, while it is 1° for HP. All these angular variations correspond to an increase of the corresponding integral, but the $dt_i/d\phi_i$ derivative is much larger for I_1 and I_2 compared to I_3 and the variation of d_i reinforces the larger variation of the first two integrals so that d_1 and d_2 decrease under constraint while d_3 remains almost constant.

3.1.4 TMTSF-anion interactions

The TMTSF cations columns and the anions in the crystal structure alternate along the $b + c$ direction at RT, HP and HPLT or along the $b/2 + c$ direction at LT. We define the mixed planes as (0 −1 1) and (0 −2 1) respectively, which contain both anions and cations. If we analyse the anion-cation interactions in terms of the distances shorter than the sum of Van der Waals radii, it appears that these interactions involve only $C(H_3)$...O distances within these planes and only one Se...O distance between adjacent planes.

In the LT structure, the surrounding of each anion is unique and very well defined because of the ordering of the anion. The distances Se...O are only slightly smaller than the sum of the Van der Waals radii (3.50 Å): 3.48 Å between O_{23} and Se_{12A} and 3.43 Å between O_{22} and Se_{12B}. These distances are similar for the 2 independent cations. The $C(H_3)$...O distances are reported in Figure 7 and we give the shortest distances between the O atoms and the

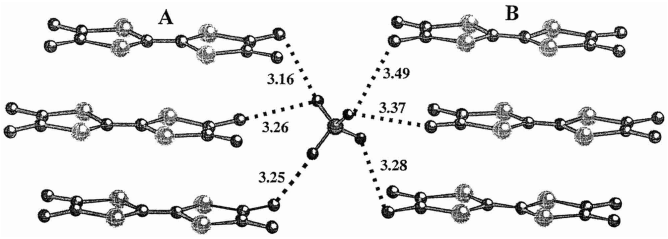

Fig. 7. View perpendicular to the TMTSF sheet plane of the anion environment showing the shortest $C(H_3)$...O distances between an anion and the A and B cations.

TMTSF cation belonging to the same (0 −2 1) plane. In these interactions, the methyl groups belong to the same side of each cation. They are shorter for the A stack with an averaged distance of 3.22 Å while the distances for the B stack are an average of 3.38 Å. This result is directly related to the analysis of the molecular geometries of A and B. We found that the differences between the methyl groups positions result in a chair-like conformation for the A TMTSF while the B cation is strictly planar. The rather short anion-A-cation contacts induce a deformation of the molecular plane through the methyl groups. In particular, the C_{17} atom of the A cation which moves away notably from the mean plane of the five-membered ring (by +0.17 Å) is associated with the shortest CH_3...O distance (3.16 Å). As this oxygen atom lies at −2.49 Å with respect to the mean plane, the corresponding interaction is repulsive. The weaker anion-B-cation interaction leads to a relatively planar cation conformation.

The evolutions of the anion-cation interactions are now analyzed when the anions remain disordered. The Se...O interactions may be measured by using two Se...O distances, each one with the adjacent anion-cation mixed planes. These distances are: 3.34 Å and 3.82 Å for RT; 3.28 Å and 3.73 Å for HP; 3.39 Å and 3.50 Å for HPLT. These distances are calculated with the disordered anion and with the Cl atom located on the inversion centre.

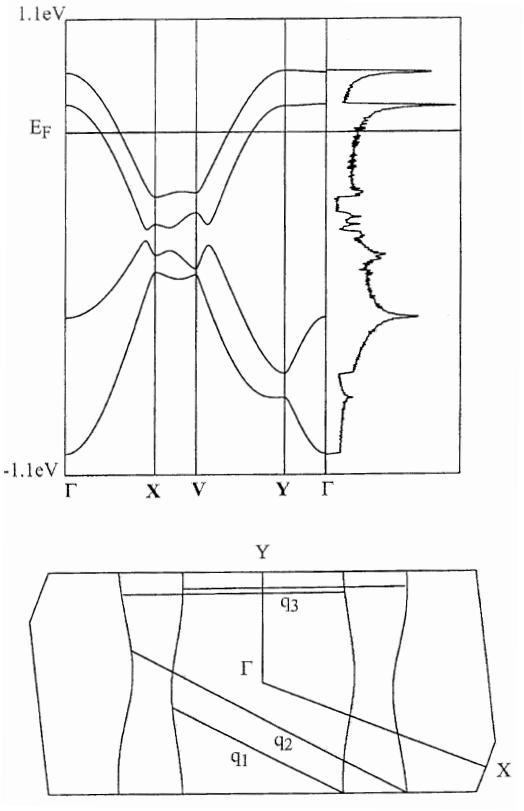

Fig. 8. Band structure and Fermi surface for the LT crystal structure.

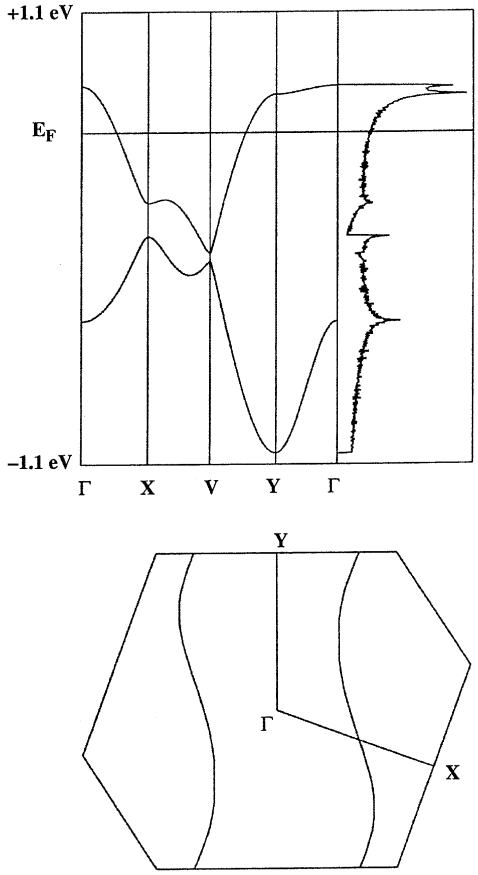

Fig. 9. Band structure and Fermi surface for the HPLT crystal structure.

The differences between the two distances are the largest for RT and HP, and they are reduced at HPLT. In the latter case, they are very close to the LT values, showing that the anion ordering does not result in a large change of the anion-cation interactions, although this ordering allows the refinement of the Cl position. These results imply that low temperature leads to a rather symmetrical environment of the anion, independent of the pressure.

3.2 Band structures and Fermi surfaces

The band structures and Fermi surfaces calculated using the LT and HPLT transfer integrals of Table 3 are given in Figures 8 and 9 respectively. The main difference between the two sets of results arise from the doubling of the unit cell along the b direction and the existence of a non-zero Δ term in the LT data. The LT band structure is characterised by the Fermi energy which cuts the two upper bands, resulting from the existence of two independent stacks. This result agrees qualitatively with previous reports [17,22]. The most important factor is the difference of the cations A and B site energies. The Δ term increases the gap between the two lines of the Fermi surface in the vicinity of the point $(2k_F, 1/6)$. The consequence of this term is to effectively increase the 1D character of the LT Fermi surface compared to the HPLT result. This result may be quantified by evaluating the different nesting vectors (see Fig. 8). The possible nestings of the Fermi surface are:

1. intraband nesting 1: $q_1 = (2k_F - 0.12, -0.11)$
2. intraband nesting 2: $q_2 = (2k_F + 0.12, -0.20)$
3. interband nesting 3: $q_3 = (2k_F, -0.37)$

These nestings are almost perfect as shown by the area of the closed orbits induced by the nesting which are much less than 1% of the area of the first Brillouin zone.

4 Conclusion

The crystal structures of $(TMTSF)_2ClO_4$ have been determined at (7 K, 1 bar) and at (7 K, 5 kbar) and compared to the room temperature (300 K, 1 bar [9]; 300 K, 6 kbar [18]) and to the previously determined LT crystal structures [15,17]. The effects of lowering the temperature is not the same as an increase of pressure.

At LT, the most important observation is that the anion ordering leads to the presence of two independent stacks of TMTSF cations. This is the only case of this ordering found in the Bechgaard salts family. The calculated

difference in the site energies of 100 meV leads to a charge transfer from the A stack to the B stack which is evaluated from the band structure calculation to be of 0.025 electron. Note that this charge transfer is not directly related to the nesting vectors q_1 and q_2 because the transfer integrals determine the 2D character of the electronic interactions. We have checked that setting the transverse t to 0 while keeping a non zero Δ gives a charge transfer closely related to the k_x component of the 1D nesting vector.

The interatomic distances of the central fragment of the organic conductors are generally used to evaluate the degree of charge transfer. In particular, a quantitative correlation was established in the case of the BEDT-TTF compounds with an accuracy of the degree of charge transfer of about 0.1 e^- [31,32]. Such a correlation does not exist for the TMTSF salts. The very small calculated charge transfer is consistent with the fact that the bond lengths of the central fragment of A and B are nearly the same. The two cations differ mainly by the methyl groups positions which result in a chair-like conformation for the A TMTSF while the B cation is strictly planar. Although the terminal carbon atoms have a little weight in the TMTSF HOMO, there is an indirect effect of the non-planarity of these carbon atoms on the dimer molecular distribution which destabilizes more the $HOMO_A$ than the $HOMO_B$.

The existence of two independent molecules in the unit cell may result from different orderings of the anions. In the low temperature crystal structure of $TMTSF_2ReO_4$, the ordering of the ReO_4 anions is (1/2, 1/2, 1/2) [33] while it is (1/2, 0, 0) in $TMTSF_2NO_3$ [34]. It is only for the particular ordering (0, 1/2, 0) of the ClO_4^- anions that the 2 independent molecules belong to 2 different stacks. The calculated Δ values are almost independent of the anion ordering: 100 meV for ClO_4^-, 110 meV for ReO_4^-, 85 meV for NO_3^-. This result confirms that the Δ term is intrinsically a molecular quantity which does not depend on the location of the independent molecules.

These values of Δ are much larger than the transition temperatures (1200 K against some tens to hundreds K). However, the EH results incorporate only a few of the different contributions to the full Hamiltonian: only the changes in the overlaps between the atomic orbitals. The EH Hamiltonian may be considered as an effective approach which does not include any of the important energetic terms as the variations of the internuclear repulsion energies or the Coulombic terms. It is clearly out of reach of this method to give even a qualitative evaluation of the anion potential.

At low temperature, independent of the pressure, the interchain transfer integrals are quite similar. Although the independence of the two columns at low temperature leads to a reverse order of the integrals on both sides of each column (I_1, I_3, I_2, I_5 *vs.* I_1, I_5, I_2, I_3), there is no significant difference between the two sets of integrals along the b direction: I_3 and I_5 are almost identical. This interpretation is confirmed by the comparison of our LT results to the previous data [15]. We have concluded that the anion ordering has no influence on the interchain interactions. The HPLT integrals are closer to the B stack LT results than to an average of the whole LT values. Moreover, the centres of mass of the low temperature crystal structures are nearly the same, independent of the pressure.

The measurements described here give us important information about the effects of the anion ordering on the differentiation of the two inequivalent stacks. We consider that further studies in the domain of solid state physics are required to fully interpret the puzzling behavior of these salts, and that the future models should incorporate this information.

We thank J.M. Fabre for providing us with the crystals of $(TMTSF)_2ClO_4$ and the Conseil Régional d'Aquitaine for financial support. We gratefully acknowledge valuable discussions with the members of the CNRS GDR 522 "Matériaux Moléculaires : du magnétisme aux supraconducteurs organiques".

References

1. D. Jérome, H. J. Schultz, Adv. Phys. **31**, 299 (1982).
2. T. Ishiguro, K. Yamaji, G. Saito, in *Organic Superconductors*, 2nd edn. (Springer-Verlag, Berlin, 1998).
3. *Advances in Synthetic Metals, Twenty years of progress in science and technology*, edited by P. Bernier, S. Lefrant, G. Bidan (Elsevier, 2000).
4. K. Bechgaard, K. Carneiro, M. Olsen, F.B. Rasmussen, C. Jacobsen, Phys. Rev. **46**, 852 (1981).
5. J.-P. Pouget, G. Shirane, K. Bechgaard, J.M. Fabre, Phys. Rev. B **27**, 5203 (1983).
6. R. Moret, J.P. Pouget, R. Comes, K. Bechgaard, J. Phys. France **46**, 1521 (1985).
7. D.U. Gubser, W.W. Fuller, T.O. Poehler, J. Stokes, D.O. Cowan, M. Lee, A.N. Bloch, Mol. Cryst. Liq. Cryst. **79**, 225 (1982).
8. S. Tomic, D. Jérome, P. Monod, K. Bechgaard, J. Phys. Lett. **43**, L839 (1982).
9. G. Rindorf, H. Soling, N. Thorup, Acta Cryst. B **38**, 2805 (1982).
10. K. Murata, L. Brossard, R. Lacoe, M. Ribault, D. Jérome, K. Bechgaard, A. Moradpour, Mol. Cryst. Liq. Cryst. **119**, 245 (1985).
11. S.S.P. Parkin, J. Voiron, R.L. Greene, Mol. Cryst. Liq. Cryst. **119**, 33 (1985).
12. F. Guo, K. Murata, H. Yoshino, S. Maki, S. Tanaka, J. Yamada, S. Nakatsuji, H. Anzai, J. Phys. Soc. Jpn **67**, 3000 (1998).
13. W. Kang, D.T. Hannahs, P.M. Chaikin, Phys. Rev. Lett. **70**, 3091 (1993).
14. D. Jérome, A. Mazaud, M. Ribault, K. Bechgaard, J. Phys. Lett. **41**, L195 (1980).
15. B. Gallois, Thèse d'État, Université Bordeaux I, 1987.
16. L. Ducasse, A. Abderrabba, B. Gallois, J. Phys. C **18**, L947 (1985).
17. L. Ducasse, A. Abderrabba, J. Hoarau, M. Pesquer, B. Gallois, J. Gaultier, J. Phys. C **19**, 3805 (1986).

18. D. Chasseau, J. Gaultier, H. Houbib, M. Rahal, L. Ducasse, High Press. Res. **7**, 41 (1991); H. Houbib, Thèse de l'Université Bordeaux I, 1988.
19. B. Gallois, J. Gaultier, C. Hauw, T. Lamcharfi, A. Filhol, Acta Cryst. B **42**, 564 (1986).
20. D. Chasseau, J. Gaultier, G. Bravic, L. Ducasse, M. Kurmoo, P. Day, Proc. R. Soc. Lond. A **442**, 207 (1993); Ph. Guionneau, J. Gaultier, M. Rahal, G. Bravic, J.M. Mellado, D. Chasseau, L. Ducasse, M. Kurmoo, P. Day, J. Mater. Chem. **5**, 1639 (1995); M. Rahal, D. Chasseau, J. Gaultier, L. Ducasse, M. Kurmoo, P. Day, Acta Cryst. B **53**, 159 (1997); Ph. Guionneau, J. Gaultier, D. Chasseau, G. Bravic, Y. Barrans, L. Ducasse, D. Kanazawa, P. Day, M. Kurmoo, J. Phys. I France **6**, 1581 (1996).
21. D. Le Pévelen, Thèse de l'Université Bordeaux I, 1999.
22. P.M. Grant, J. Phys. Colloq. France **44**, C3-847 (1983).
23. T. Mori, A. Kobayashi, Y. Sasaki, H. Kobayashi, G. Saito, H. Hinokuchi, Bull. Chem. Soc. Jpn **57**, 627 (1984).
24. M.-H. Whangbo, J. Ren, W. Liang, E. Canadell, J.-P. Pouget, S. Ravy, J.M. Williams, M.A. Reno, Inorg. Chem. **31**, 4169 (1992).
25. J.D. Martin, M.-L. Doublet, E. Canadell, J. Phys. I France **3**, 2451 (1993).
26. J.M. Delrieu, M. Roger, Z. Toffano, A. Moradpour, K. Bechgaard, J. Phys. France **47**, 839 (1986); T. Takahashi, Y. Maniwa, H. Kawamura, G. Saito, J. Phys. Soc. Jpn **53**, 1364 (1986).
27. S. Ishibashi, A.A. Manuel, M. Kohyama, J. Phys. Cond. Matt. **11**, 2279 (1998).
28. R.V. Kasowski, M.-H. Whangbo, Inorg. Chem. **29**, 360 (1990).
29. The exponents, contraction coefficients and atomic parameters are: 3.137, 1.890, 0.58284, 0.48513 and −20.5 eV for Se 4*s*; 2.715, 1.511, 0.53465, 0.55536 and −14.0 eV for Se 4*p*; 1.813, 1.153, 0.76135, 0.26322 and −21.4 eV for C 2*s*; 2.730, 1.257, 0.25951, 0.80253 and −11.4 eV for C 2*p*; 1.300, 1.000 and −13.06 eV for H 1*s*.
30. A. Abderrabba, Thèse d'État, Université Bordeaux I, 1987.
31. P. Guionneau, C.J. Kepert, G. Bravic, D. Chasseau, M.R. Truter, M. Kurmoo, P. Day, Synth. Metals **85**, 1973 (1997).
32. P. Guionneau, D. Chasseau, J.A.K. Howard, P. Day, Acta Cryst. C **56**, 453 (2000).
33. G. Rindorf, H. Soling, N. Thorup, Acta Cryst. C **40**, 1137 (1984).
34. S. Hébrard-Bracchetti, Thèse de l'Université Bordeaux I, 1996.